Journal of Photochemistry and Photobiology A: Chemistry 203 (2009) 92–99

Contents lists available at ScienceDirect

Journal of Photochemistry and Photobiology A: Chemistry

journal homepage: www.elsevier.com/locate/jphotochem

A density functional theory study on photophysical properties of red light-emitting materials: Meso-substituted porphyrins

Xue-feng Ren[a], Ai-min Ren[a,*], Ji-kang Feng[a,b], Chia-chung Sun[a]

[a] State Key Laboratory of Theoretical and Computational Chemistry, Institute of Theoretical Chemistry, Jilin University, Changchun 130023, People's Republic of China
[b] The College of Chemistry, Jilin University, Changchun 130023, People's Republic of China

ARTICLE INFO

Article history:
Received 21 June 2008
Received in revised form
26 November 2008
Accepted 29 December 2008
Available online 7 January 2009

Keywords:
Porphyrin
Ionization potential
Electron affinity
Reorganization energy

ABSTRACT

The density functional theory (DFT) has been applied to investigate the photophysical properties of meso-substituted porphyrins: 5,15-difluorenylporphyrin (DFP), 5,10,15,20-tetrafluorenylporphyrin (TFP), Zn-5,10,15,20-tetrafluorenylporphyrin (FPZ) and Zn-5,10,15,20-tetrafluorenoneporphyrin (OPZ). The geometry structures, frontier molecular orbitals, ionization potential (IP), electron affinity (EA) and reorganization energy (λ) together with the absorption and emission wavelengths of these compounds were investigated. Theoretical calculations indicated that the introduction of meso-substitutions brought about significant effect on the photophysical properties. The TFP molecule has lowest hole injection energy barrier of all the studied compounds, and OPZ owns lowest electron injection energy barrier of them. The equilibrium of the hole and electron transport of FPZ is better than those of porphyrin (FBP), DPZ, TFP, and OPZ. The electron reorganization energies ($\lambda_{electron}$) of FBP, DFP, TFP, FPZ and OPZ are 0.22 eV, 0.20 eV, 0.23 eV, 0.26 eV and 0.13 eV, respectively, which are smaller than tris(8-hydroxyquinolinato) aluminum(III), thus these molecules are potential electron transport materials. Their visible absorption wavelengths are calculated by TD-B3LYP and semi-empirical ZINDO methods, and these results agree with corresponding experimental values. The fluorescence spectra of these complexes predicted by TD-HF method exhibit more consistent results with experimental data than by TD-B3LYP method.

1. Introduction

Since the early work of Tang and VanSlyke [1], organic light-emitting diodes (OLEDs) have attracted tremendous attention in application to the large-area flat-panel display devices. Normally, OLED devices are comprised by three layers: the electron transport layer, the emitter layer, and hole transport layer. Holes are injected from anode into the hole transport layer then migrate toward emitter layer, while electrons are injected from cathode into the electron transport layer then migrate toward emitter layer. Once they recombine in the emitter layer, the excitons are produced. Therefore, the balance of charge-carrier transport rate is very important for high efficiency OLEDs.

Nowadays, a new type of nondopant red light-emitting materials has emerged [2–6], in which 5,15-difluorenylporphyrin (DFP), 5,10,15,20-tetrafluorenylporphyrin (TFP), Zn-5,10,15,20-tetrafluorenylporphyrin (FPZ) and Zn-5,10,15,20-tetrafluorenoneporphyrin (OPZ) (as depicted in Fig. 1) reported by Paul-Roth [5,6] exhibit good red chromaticity and enhanced emission efficiency, as well as higher fluorescence quantum yield than many other porphyrins [7] and Zn porphyrins [8]. However, there has been no report on the efficiency of carrier injection and transport properties. And it is also uncertain whether these compounds can function as electron transport materials (ETM), hole transport materials (HTM) or emitter materials (EM). Therefore, this contribution will present a systematical theoretical investigation on the electronic structures, electronic spectra, especially for the charge injection and transport properties of DFP, TFP, FPZ and OPZ. We calculated the ionization potential (IP) and electronic affinity (EA) to evaluate the energy barrier for injection holes and electrons, and also computed reorganization energy (λ) to investigate the charge transport on the Marcus electron transfer theory [9]. And all the calculated values were compared with the attainable experimental data to testify the theoretical methods.

2. Computational methods

Density functional theory (DFT) has been widely used in π-conjugated systems including porphyrins, and these results are more accurate than those derived from other methods [10–13]. It is known that due to the self-interaction error in DFT and subsequent wrong asymptotic behavior of the potential, in quantitative terms, DFT orbital energies are in much poorer agreement with photoelectron spectra than HF IPs by Koopmans Theory. However, DFT

* Corresponding author. Tel.: +86 431 88499856; fax: +86 431 88945942.
E-mail address: aimin.ren@gmail.com (A.-m. Ren).

1010-6030/$ – see front matter © 2009 Elsevier B.V. All rights reserved.
doi:10.1016/j.jphotochem.2008.12.028

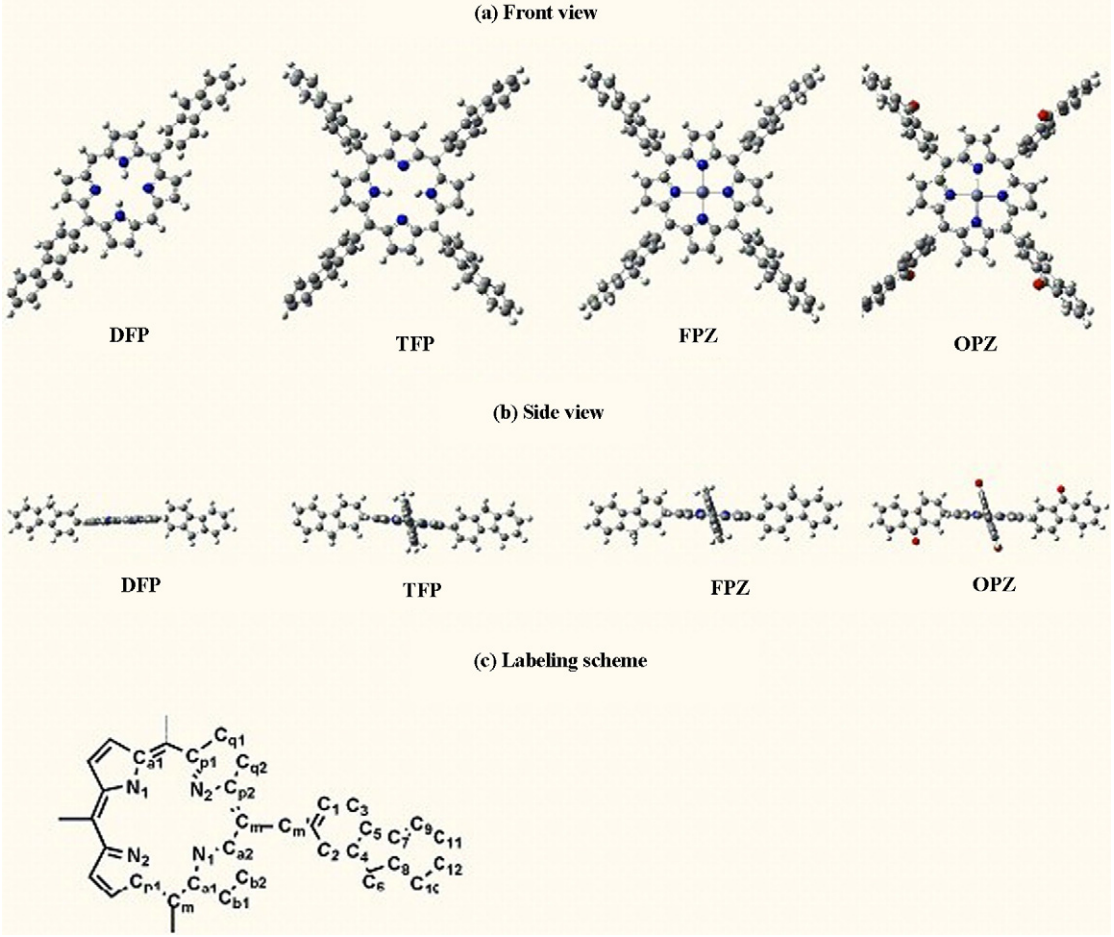

Fig. 1. (a) Front view of the optimized structures of DFP, TFP, FPZ and OPZ obtained by DFT//B3LYP/6-31G(d); (b) side view of them; (c) labeling scheme for all the meso substituted-porphyrins (especially for FPZ and OPZ, Zn is connected with N_1 and N_2 in the center of porphyrin).

can excellently predict to the lowest energy state as well as the IP and EA by ΔSCF method (i.e. IP/EA value is obtained by the energy difference between the cationic/anionic and neutral states). Thus all the geometries optimization of these compounds in their neutral, cationic and anionic states were calculated by Beck's three parameters hybrid functional (B3LYP) [14–16] with 6-31G(d) basis sets. The neutral, cationic and anionic forms of these compounds were used to compute the IP and EA, hole extraction potentials (HEP), electron extraction potentials (EEP) and reorganization energy (λ). On the basis of the optimized ground state geometries, the electronic absorption spectra were investigated by the TD-B3LYP and ZINDO [17] methods. Considering the large size of these molecules and available computational resources, the lowest singlet excited state structures were calculated with ab initio CIS/3-21G(d). Following these optimized excited structures, the fluorescence spectra were calculated by the TD-HF and TD-B3LYP methods. All the above calculations were performed on the SGI origin 2000 server, using Gaussian03 program package [18].

3. Results and discussion

3.1. Neutral and ionic geometry structures

The molecular structures and atoms labeling scheme are depicted in Fig. 1, and main optimized geometry structural parameters are collected in Table 1. Compared with porphyrin (FBP), the introductions of fluorenyl and fluorenone fragments have slightly drawn C_m away from porphyrin core, which result in lengthened $C_{\alpha1}$—C_m, $C_{\alpha2}$—C_m, C_{p1}—C_m and C_{p2}—C_m bond lengths. Table 1 also shows that the main structure parameters of DFP are similar with TFP. The maximum deviations are found in the $C_{\alpha2}$—C_m, C_{p2}—C_m bond lengths. And OPZ has similar geometrical and electronic structures with FPZ. According to the NBO analyses, the charge population of fluorenyl and fluorenone are 0.0148 and 0.0164 a.u., respectively, which indicates that the ability of electron-donation of fluorenyl is similar with that of fluorenone. After Zn atom is chelated at the pyrrole ring, the bond lengths in porphyrin ring have changed. The C_{a1}—C_{b1}, C_{a2}—C_{b2}, C_{p1}—N_2, C_{p2}—N_2 bond lengths of FPZ increase by about 0.010 Å than those of TFP, and C_{p1}—C_{q1}, C_{p2}—C_{q2} bond lengths of FPZ decrease by about 0.015 Å than those of TFP.

From side view of the studies molecules, the porphyrin rings are near in plane. Since the repulsion of hydrogen's between C_{q1}—H/C_{b1}—H and C_1—H/C_2—H, the dihedral angles a(C_1—$C_{m'}$—C_m—C_{a2}) between substitutions plane (fluorenyl or fluorenone) and porphyrin-ring plane are 61.9°, 67.8°, 69.1°, 68.6° for DFP, TFP, FPZ, OPZ, respectively. The large inter-angles are considered as the structural feature of energy-transfer systems [19].

The bond lengths deviations between the ionic and its corresponding neutral states are drawn in Fig. 2. It is clear that the larger variations in different states mainly focus on porphyrin ring. As shown in Fig. 2, for DFP, in the cationic state, the inter-ring distance $C_{m'}$—C_m (labeled 15) decreases by 0.020 Å and the C_{a1}—C_m (labeled 5) increases by 0.013 Å. In the anionic state, the inter-ring distance $C_{m'}$—C_m decreases by 0.015 Å, and C_{p2}—N_2 (labeled 11) and C_{p2}—C_m (labeled 13) increase by 0.015 Å. Similarly, for TFP, in

Table 1
Selected bond lengths (Å) for porphyrin (FBP), DFP, TFP, FPZ and OPZ, and bond angles (°) for porphyrin relatives.

	Bond length (Å)						Bond angles (°)			
	FBP	DFP	TFP	FPZ	OPZ		DFP	TFP	FPZ	OPZ
C_{a1}—C_{b1}	1.435	1.436	1.434	1.445	1.445	$\alpha(C_{a1}—C_m—C_{p1})$	123.3	125.3	124.7	124.9
C_{a2}—C_{b2}	1.435	1.433	1.434	1.455	1.445	$\alpha(C_{a2}—C_m—C_{p2})$	129.4	125.3	124.7	124.9
C_{a1}—N_1	1.373	1.375	1.377	1.377	1.377	$\alpha(C_{b1}—C_{a1}—C_m)$	128.5	126.7	124.3	124.4
C_{a2}—N_1	1.373	1.373	1.377	1.377	1.377	$\alpha(C_{p1}—N_2—C_{p2})$	105.6	110.7	106.5	106.5
$C_{\alpha1}$—C_m	1.394	1.408	1.406	1.407	1.407	$\alpha(C_{a1}—N_1—C_{a2})$	110.8	119.0	106.5	106.5
C_{a2}—C_m	1.394	1.394	1.406	1.407	1.407	$\alpha(C_1—C_{m'}—C_m—C_a)$	61.9	67.8	69.1	68.6
C_{p1}—C_{q1}	1.460	1.462	1.460	1.445	1.445					
C_{p2}—C_{q2}	1.460	1.457	1.460	1.445	1.445					
C_{p1}—N_2	1.363	1.366	1.367	1.378	1.377					
C_{p2}—N_2	1.363	1.363	1.367	1.378	1.377					
C_{p1}—C_m	1.400	1.415	1.412	1.407	1.406					
C_{p2}—C_m	1.400	1.399	1.412	1.407	1.406					
$C_{m'}$—C_m		1.494	1.498	1.499	1.498					
N_1—Zn				2.043	2.043					

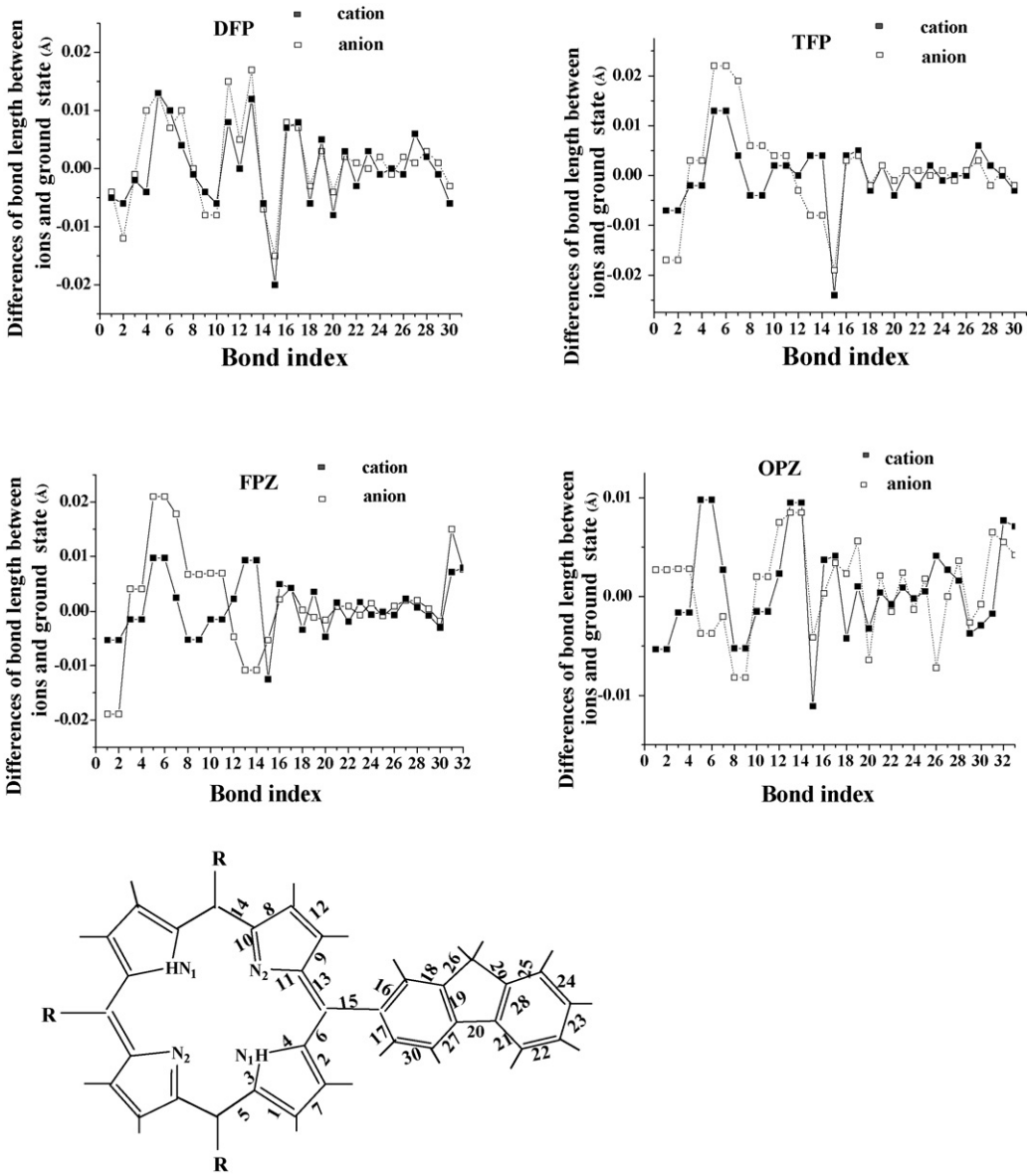

Fig. 2. The bond lengths changes between the ionic and neutral states of DFP, TFP, FPZ, OPZ are drawn in line, and the bond index are labeled behind (For FPZ, the labeled 31 and 32 bond lengths are Zn—N_1 and Zn—N_2, respectively. For OPZ, the labeled 31, 32, 33 bond lengths are C=O, Zn—N_1, Zn—N_2, respectively).

Table 2
Molecular orbtial energy levels (eV) of substituted porphyrins.

		L+2	L+1	L	H	H−1	H−2		L+2	L+1	L	H	H−1	H−2
Energy	DFP	−0.94	−2.17	−2.24	−4.94	−5.24	−5.82	TFP	−0.92	−2.16	−2.17	−4.83	−5.17	−5.78
Energy	FPZ	−0.89	−2.09	−2.10	−4.91	−5.11	−5.76	OPZ	−2.31	−2.38	−2.49	−5.21	−5.37	−6.23

L+2 and L+1 represent LUMO+2 and LUMO+1 orbtials, and H and H−1 represent HOMO and HOMO−1 orbtials, etc.

the cationic state, the C_{a1}—C_m (labeled 5), C_{a2}—C_m (labeled 6) and $C_{m'}$—C_m (labeled 15) bond lengths increase by 0.013 Å, 0.013 Å and 0.024 Å, respectively. In the anionic state, the C_{a1}—C_{b1} (labeled 1), C_{a2}—C_{b2} (labeled 2), $C_{m'}$—C_m (labeled 15) bond lengths decrease by about 0.017 Å, and C_{a1}—C_m (labeled 5) and C_{a2}—C_m (labeled 6) bond lengths increase by 0.022 Å. And for FPZ, in the cationic state, the C_{a2}—C_m (labeled 13) and C_{p2}—C_m (labeled 14) bond lengths increase by 0.01 Å, and the $C_{m'}$—C_m (labeled 15) bond distance shortens by 0.012 Å. In the anionic state, the C_{a1}—C_m (labeled 5) and C_{a2}—C_m (labeled 6) distances increase 0.020 Å, the C_{a1}—C_{b1} (labeled 1) and C_{a2}—C_{b2} (labeled 2) distances decrease 0.020 Å. For OPZ, the bond deviations between the ionic and neutral states are lesser than 0.010 Å, except for $C_{m'}$—C_m (decreases 0.011 Å in the cationic state).

3.2. Frontier molecular orbitals and charge injection and transport

To shed light on the chemical activity of porphyrins, energies of the frontier orbital are listed in Table 2. And the contour plots of these orbitals are illustrated in Fig. 3. As listed in Table 2, the LUMOs and LUMO+1s orbitals of studied molecules are nearly degenerate, and they are separated from other unoccupied orbitals (excepting for OPZ). However, the HOMOs and HOMO−1s orbitals of them are not degenerate any longer. These characteristics are not entirely consistent with the most common Gouterman four-orbital model [20]. Table 2 also shows that the energies of HOMO increase in following order: OPZ < DFP < FPZ < TFP, indicating that the introduction of fluorenyl at meso-position further enhance the hole injection performance. And the order of LUMO energies decrease as FPZ > TFP = DFP > OPZ, which suggests that the cooperation with fluorenone enhance the electron injection ability. As shown in Fig. 3, all these frontier orbitals own π characteristics. And the electronic populations of these orbitals mainly spread over porphyrin ring (excepting for the LUMO of OPZ), indicating that the substitution of fluorenyl and fluorenone do not significantly change the four-orbital distribution.

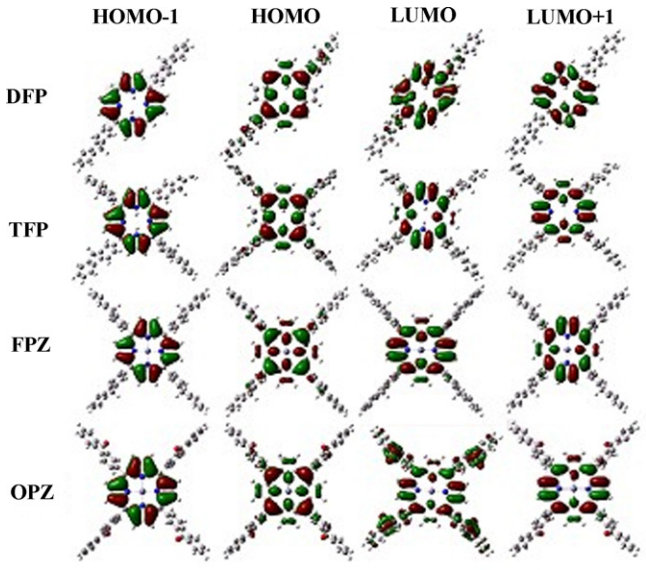

Fig. 3. Electron density distributions of frontier molecular orbitals of DFP, TFP, FPZ and OPZ.

As well known, efficient charge injection and transport rates are important parameters for OLEDs. In view of this, ionization potential and electronic affinity are used to evaluate the energy barrier for injection holes and electrons. The calculated results are listed in Table 3. As shown in Table 3, the order of IP values decrease as follow: FBP > OPZ > DFP > FPZ > TFP, and EA increase in the follow orders: FBP ≈ FPZ < DFP < TFP < OPZ. It is obvious that the abilities of creation holes and electrons are increased by introduction of meso-substitutions (fluorenyl and fluorenone). Normally, the lower IP value of the hole-transport layer (HTL), the easier the entrance of holes from ITO to HTL; and the higher EA value of the electron-transport layer (ETL), the easier the entrance of electrons from cathode to ETL. Hence, TFP and OPZ are good holes and electrons injection materials, respectively, which are consistent with the indication from the energies analysis of their HOMOs and LUMOs.

The charge mobility in organic materials are usually described with Marcus electron transfer theory [9], in which the charge transport in the organic solid can be viewed as electron hopping model. The rates of charge transfer can be approximately described as:

$$K_{\text{hole/electron}} = \frac{4\pi^2}{h}\Delta H_{ab}^2 \frac{1}{\sqrt{4\pi\lambda_{\text{hole/electron}}T}} \exp\left(-\frac{\lambda_{\text{hole/electron}}}{4K_bT}\right) = A \exp\left(-\frac{\lambda_{\text{hole/electron}}}{4K_bT}\right) \quad (1)$$

where T is the temperature, K_b is the Boltzmann constant, H_{ab} is electronic coupling matrix element. H_{ab} lies on the center distance between the donator and acceptor. Normally, intermolecular charge transfer range in noncrystal is very narrow, and its magnitude is very limited [21], thus H_{ab} will be considered to be a constant in this work. Hence, according to the analysis above, the efficient charge transfer largely relies on the $\lambda_{\text{hole}}/\lambda_{\text{electron}}$. The $\lambda_{\text{hole}}/\lambda_{\text{electron}}$ is hole/electron reorganization energy, which can be defined as [22] and be calculated as follows:

$$\lambda_{\text{hole}} = \lambda_+ + \lambda_1 = [E^+(\text{A}) - E^+(\text{A}^+)] + [E(\text{A}^+) - E(\text{A})] = \text{IP(v)} - \text{HEP} \quad (2)$$

$$\lambda_{\text{electron}} = \lambda_- + \lambda_2 = [E^-(\text{A}) - E^-(\text{A}^-] + [E(\text{A}^-) - E(\text{A})] = \text{EEP} - \text{EA(v)} \quad (3)$$

Table 3
Ionization potential (IP), electron affinity (EA), extraction potentials (EP), and reorganization energy (λ) for each molecule (in eV) calculated by DFT//B3LYP/6-31G(d).

Molecule	IP (v)	IP (a)	HEP	λ_{hole}	EA (v)	EA (a)	EEP	$\lambda_{\text{electron}}$
FBP	6.48	6.45	6.42	0.06	0.87	0.99	1.09	0.22
DFP	5.97	5.88	5.80	0.17	1.17	1.27	1.37	0.20
TFP	5.73	5.62	5.54	0.19	1.20	1.32	1.43	0.23
FPZ	5.86	5.70	5.61	0.25	1.07	1.22	1.33	0.26
OPZ	6.11	6.01	5.93	0.18	1.67	1.75	1.80	0.13

The suffixes (v) and (a) indicate vertical and adiabatic values, respectively.

Table 4
The absorption spectra of DFP, TFP, FPZ and OPZ calculated by TDDFT and ZINDO methods, together with the experimental data [5,6].

TDDFT				ZINDO			Experiment
	Wavelength (nm)	f	Main configuration		Wavelength (nm)	f	Wavelength (nm)
(a) DFP							
S_1	567.5	0.0446	38%(H → L+1) 26%(H−1 → L) 26%(H → L)	S_1	765.0	0.0070	633 and 577
S_2	533.3	0.0904	39%(H → L) 22%(H → L+1)	S_2	676.6	0.0087	541 and 505
S_3	397.6	1.5468	39%(H−3 → L) 28%(H−1 → L+1)	S_3	406.2	3.6999	411
S_4	386.2	0.3657	28%(H−1 → L) 23%(H−3 → L+1)	S_4	392.0	1.9809	
S_7	373.4	0.0915	32%(H−3 → L+1) 30%(H−3 → L)	S_8	327.4	0.5801	
S_9	359.6	0.4325	35%(H−3 → L+1)	S_{11}	307.7	0.0828	
S_{12}	340.5	0.5494	58%(H−5 → L)	S_{13}	301.7	0.0618	
S_{13}	331.0	0.2679	51%(H−5 → L+1)	S_{14}	299.5	0.1408	
S_{14}	322.3	0.3698	45%(H → L+3)	S_{17}	290.1	0.1214	
				S_{19}	286.8	0.0164	
				S_{20}	282.2	0.1766	
				S_{23}	279.9	0.0929	265–300
				S_{24}	276.2	0.0354	
				S_{28}	270.3	0.0577	
				S_{33}	257.6	0.1637	
				S_{35}	253.9	0.0557	
				S_{37}	252.0	0.0388	
				S_{38}	251.1	0.0674	
				S_{40}	249.4	0.0471	
				S_{42}	243.6	0.0408	
(b) TFP							
S_1	583.6	0.0454	67%(H → L+1) 38%(H−1 → L)	S_1	792.2	0.0016	649 and 593
S_2	547.7	0.1143	35%(H−1 → L+1) 63%(H → L)	S_2	698.5	0.0051	557 and 519
S_3	407.4	1.3522	37%(H−1 → L) 13%(H → L+1)	S_3	418.2	3.2691	
S_4	398.4	1.4742	25%(H−5 → L) 36%(H−1 → L+1)	S_4	415.6	3.5352	425
S_8	383.4	0.0358	96%(H−4 → L+1)	S_8	335.6	0.5545	
S_{10}	381.1	0.0150	87%(H−4 → L)	S_{11}	320.3	0.0818	
S_{13}	364.7	0.2872	63%(H−5 → L) 11%(H−7 → L)	S_{12}	314.2	0.0333	
S_{16}	346.7	0.3764	74%(H → L+3) 19%(H−7 → L+1)	S_{15}	306.0	0.1329	
S_{17}	343.5	0.2818	76%(H−7 → L) 14%(H → L+5)	S_{16}	304.3	0.1309	
S_{19}	335.1	0.4961	43%(H−7 → L+1) 21%(H → L+3)	S_{17}	303.6	0.0314	
S_{20}	332.6	0.0773	74%(H → L+5)	S_{18}	301.6	0.0180	
S_{23}	315.1	0.0664	98%(H−1 → L+3)	S_{20}	299.7	0.0417	
				S_{25}	290.1	0.0814	
				S_{30}	285.4	0.0603	
				S_{33}	281.0	0.0603	
				S_{34}	280.3	0.1168	
				S_{36}	278.2	0.0473	
				S_{41}	272.1	0.1021	
				S_{43}	269.7	0.0551	268
				S_{47}	258.7	0.1253	
				S_{49}	256.6	0.0870	
				S_{51}	255.2	0.0914	
				S_{53}	253.8	0.0559	
				S_{56}	251.1	0.0341	
(c) FPZ							
S_1	540.6	0.0455	60%(H → L) 42%(H−1 → L+1)	S_1	705.2	0.0003	594 and 552
S_2	540.6	0.0356	60%(H → L+1) 42%(H−1 → L)	S_2	704.9	0.0005	
S_3	398.7	1.4461	32%(H−1 → L) 20%(H−5 → L+1)	S_3	409.8	3.3905	428
S_4	396.7	1.5553	33%(H−1 → L+1) 21%(H−5 → L)	S_4	408.9	3.5093	
S_8	377.3	0.0025	96%(H−4 → L+1)	S_8	316.0	0.0290	
S_{11}	375.9	0.0036	92%(H−4 → L)	S_9	315.8	0.0809	
S_{13}	355.9	0.3818	72%(H−5 → L)	S_{12}	303.2	0.2206	
S_{14}	355.4	0.4506	72%(H−5 → L+1)	S_{14}	302.8	0.2359	
S_{17}	336.0	0.0389	53%(H−7 → L+1) 39%(H → L+3)	S_{18}	299.1	0.1135	
S_{18}	335.2	0.0645	77%(H−7 → L)	S_{19}	298.9	0.1585	
S_{20}	332.3	0.0227	51%(H → L+3) 36%(H−7 → L+1)	S_{24}	290.3	0.0048	
				S_{25}	288.3	0.0301	
				S_{26}	287.4	0.0160	
				S_{29}	286.5	0.0007	
				S_{30}	285.9	0.0093	
				S_{33}	278.2	0.0006	
				S_{34}	277.3	0.0083	
				S_{37}	276.0	0.0644	
				S_{39}	275.3	0.0823	
				S_{47}	256.1	0.1472	263
				S_{48}	255.8	0.1694	
				S_{50}	252.1	0.0236	
				S_{51}	251.8	0.0499	
				S_{52}	251.5	0.1417	
				S_{55}	250.7	0.1506	
				S_{58}	248.0	0.0173	

Table 4 (*Continued*)

TDDFT				ZINDO			Experiment
Wavelength (nm)		f	Main configuration	Wavelength (nm)		f	Wavelength (nm)
				S_{62}	244.1	0.0944	
				S_{63}	243.9	0.1902	
				S_{64}	241.1	0.0511	
				S_{65}	241.0	0.0011	
				S_{68}	238.0	0.0524	
				S_{69}	237.7	0.0269	
(d) OPZ							
S_1	550.3	0.0557	66%(H → L) 33%(H−1 → L+1)	S_1	704.5	0.0020	599 and 556
S_2	543.6	0.0173	54%(H → L+1) 43%(H−1 → L)	S_2	703.1	0.0008	
S_4	492.1	0.0305	98%(H → L+3)	S_3	449.1	0.0021	
S_6	482.8	0.0722	68%(H → L+5)	S_5	449.0	0.0004	
S_7	460.2	0.0243	99%(H−1 → L+3)	S_7	413.4	3.0113	431
S_{10}	458.7	0.2240	52%(H−1 → L+5) 36%(H−1 → L)	S_8	412.5	3.1764	
S_{11}	397.1	0.0658	21%(H−11 → L+3) 20%(H−10 → L+2) 20%(H−12 → L+4)	S_{11}	381.8	0.3094	
S_{12}	396.9	0.0292	21%(H−10 → L+4) 21%(H−12 → L+2) 21%(H−13 → L+3)	S_{12}	381.0	0.3378	
S_{15}	393.1	0.6233	21%(H−4 → L) 15%(H−2 → L+4) 15%(H−3 → L+2)	S_{15}	335.8	0.0104	
S_{16}	392.2	0.7641	18%(H−5 → L) 13%(H → L+5) 13%(H−1 → L+1)	S_{16}	334.4	0.0060	
S_{19}	384.3	0.7657	17%(H−1 → L+1) 12%(H−4 → L+3) 12%(H−2 → L+2) 12%(H−3 → L+4)	S_{20}	325.2	0.0005	
				S_{21}	324.2	0.0197	
				S_{24}	308.5	0.0200	
				S_{25}	308.4	0.0427	
				S_{30}	298.5	0.0048	
				S_{31}	297.9	0.0069	
				S_{34}	292.2	0.0198	
				S_{36}	292.0	0.0042	
				S_{37}	290.5	0.0634	
				S_{39}	289.6	0.0072	
				S_{42}	277.9	0.0947	
				S_{43}	277.8	0.0575	
				S_{45}	276.2	0.0005	
				S_{46}	275.9	0.0559	
				S_{49}	273.4	0.1290	
				S_{51}	272.3	0.1094	
				S_{59}	258.7	1.4428	260
				S_{60}	257.9	1.1607	
				S_{62}	254.0	0.4031	
				S_{63}	253.4	0.3606	
				S_{65}	250.1	0.0992	
				S_{68}	248.8	0.9756	
				S_{69}	245.4	0.2389	
				S_{70}	244.4	0.2095	

E^+, E and E^- represent the energies of the cation, neutral and anion species in their lowest energy geometries, respectively, while (A^+), (A) and (A^-) denote the structures of them. $E^{+/-}$(A) is the energy of cation/anion calculated with the optimized structure of the neutral molecule A, and so on. λ_+ is the relaxation energies of a natural molecule A captured an hole going toward A^+ optimum geometry on the potential energy surface of A^+. And λ_1 is the relaxation energies from A^+ extracted an hole going toward A optimum geometry on the potential energy surface of A. The sum of λ_+ and λ_1 is the hole reorganization energy λ_{hole}. Similarly, in the electron transport process, $\lambda_{electron} = \lambda_- + \lambda_2$. In terms of above calculated model, the calculated λ_{hole} and $\lambda_{electron}$ are listed in Table 3. Table 3 shows that the λ_{hole} and $\lambda_{electron}$'s values of FBP are not in the same magnitude, the imbalance of charge-carrier transport rates results in the low luminous efficiency. By adding the substitutions of fluorenyl and fluorenone into FBP, the λ_{hole} and $\lambda_{electron}$'s values are regulated to near same magnitude, which will effectively increase the probability of confined excitons in the light-emitting layer. As listed in Table 3, FPZ has the better equal rates of hole and electron transport than FBP, DPZ, TFP, and OPZ. The electron reorganization energies ($\lambda_{electron}$) of FBP, DFP, TFP, FPZ and OPZ are 0.22 eV, 0.20 eV, 0.23 eV, 0.26 eV and 0.13 eV, respectively, which are smaller than tris(8-hydroxyquinolinato)aluminum(III) [23] (the most extensively used electron transport materials in OLEDs), thus these molecules are potential electron transport materials.

3.3. Electronic spectrum

TDDFT//B3LYP/6-31G(d) is employed to calculate the absorption spectra of DFP, TFP, FPZ and OPZ. Considering semi-empirical ZINDO method can also successfully predict the electronic spectra properties for the series of porphyrins [24–27], thus ZINDO method is used to predict these absorption spectra in this work. On the basis of the calculation results (Table 4), simulated the electronic absorption spectra are drawn in Fig. 4. Considering relative weak intensity of Q-bands spectra are not easily detected, we have magnified this part in Fig. 4 too.

As shown in Fig. 4, the Q bands for DFP, TFP, FPZ, OPZ calculated by TDDFT are in the centre of 550 nm (as listed in Table 4, 567 and 533.3 nm for DFP, 547.7 nm for TFP, 540.6 nm for FPZ, and 550.3 nm for OPZ), while the Q bands for them calculated by ZINDO are above 650 nm. The experimentally observed Q bands of them are in the 500–700 nm range. The calculated results suggest that the absorption bands in 540–590 nm and 650–800 nm calculated by TDDFT and ZINDO consist with the part of the experiment absorption bands, respectively. As listed in Table 4, the main transition orbtials for these Q bands are HOMOs, HOMO−1s, LUMOs, and LUMO+1s. From the charge density distribution analysis (Fig. 3), we can conclude that the electron transfer for Q bands of DFP, TFP, FPZ, OPZ are focus on the porphyrin fragment.

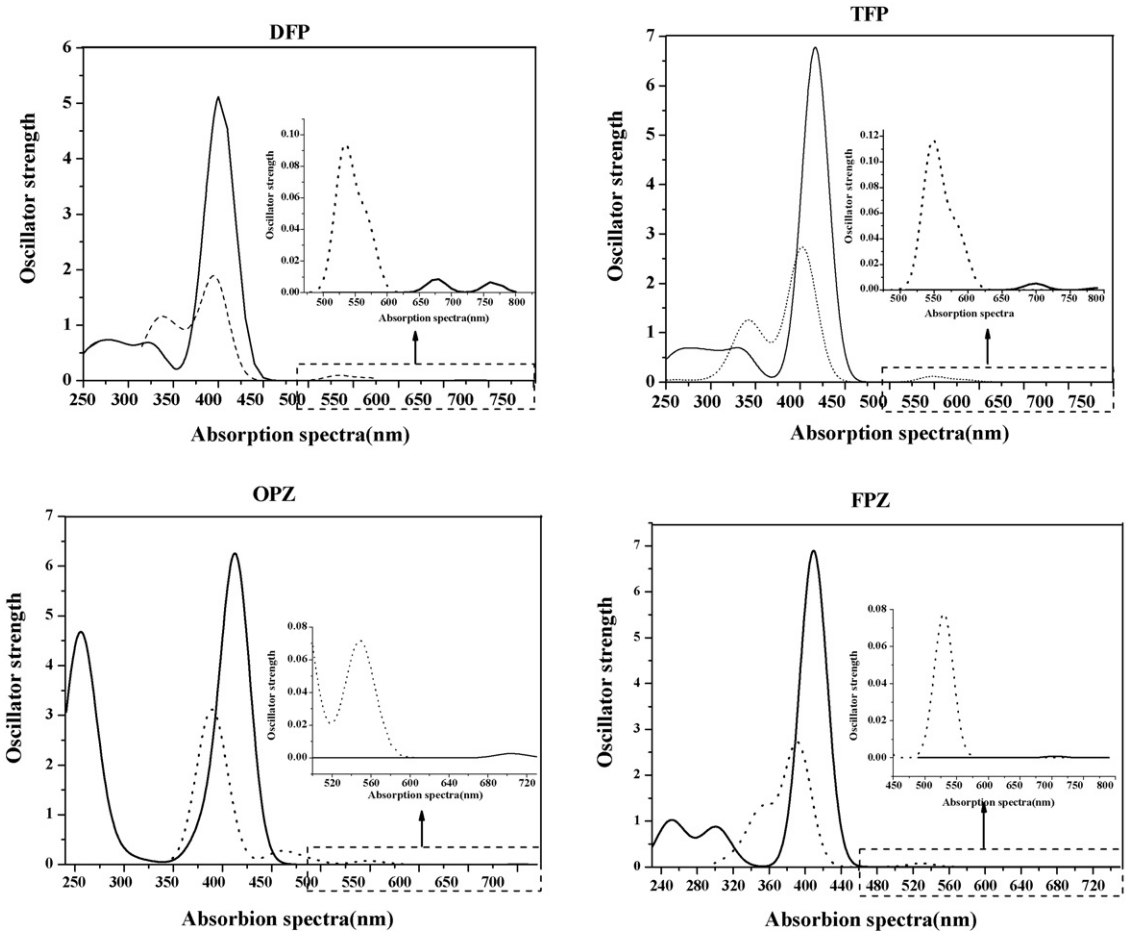

Fig. 4. Simulated the electronic absorption spectra of DFP, TFP, FPZ and OPZ with the calculated data by TDDFT/B3LYP/6-31G* (in dote line) and ZINDO (in line).

For intense B bands absorption peak, as listed in Table 4, the results calculated by TDDFT (and ZINDO) are 397.6 (406.2 and 392.0 nm), 407.4 and 398.4 nm (418.2 and 415.6 nm), 398.7 and 396.7 nm (409.8 and 408.9 nm), 392.2 and 384.3 nm (413.4 and 412.5 nm), for DFP, TFP, OPZ and FPZ, respectively, and the experimental values for them are 411, 425, 431, 428 nm in the same order. It is clear that the calculated results by ZINDO and TDDFT methods are in agreement with the experiment values. Considering the computations of such wider spectra band (from 250 to 600 nm) by TDDFT will demand huge computer time, thus ZINDO method is applied to investigate the absorption spectra. From the analysis of transition orbitals (Table 4), we find that HOMOs, HOMO−1s, LUMOs, and LUMO+1s for DFP, TFP, OPZ and FPZ play important roles in these B bands. In addition, the HOMO-3 of DFP, HOMO-5 of TFP and FPZ, HOMO-5, HOMO-4, HOMO-3, HOMO-2 of OPZ also play roles in these B bands. And by the electron density analysis, we find that these inner molecular orbitals are located on substitutions. Hence, the main electron transitions of B bands for DFP, TFP, OPZ and FPZ, are assigned to be from porphyrin to porphyrin, and from substitutions to porphyrin.

In the high energy absorption region (higher than B bands), there are broad absorption bands from 260 to 350 nm for DFP and TFP. And there are two broad absorption bands from 240 to 270 nm and from 270 to 330 nm for FPZ. All of these spectra cover with the fluorene absorption (268.0 nm [5,6]) and fluorescence spectra (around 300 nm [5,6]). It indicates that fluorene has been excited and the excited energy is absorbed by DFP, TFP and FPZ directly instead of its emission. Similarly, for OPZ, there is broad absorption spectrum from 240 to 330 nm, which covers with the fluorenone absorption (around 260 nm [5,6]) and fluorescence spectra (around 300 nm [5,6]). In conclusion, the experimental observations of the spectra overlap between the donor fluorescence (fluorene and fluorenone) and the acceptor absorption (DFP, TFP, FPZ and OPZ) spectra have been detected in theory.

The excited-state properties of DFP, TFP, FPZ, and OPZ were fully optimized using CIS/3-21G(d). Since the structural differences between the ground and excited state geometries can indicate the parts of the molecule involved in light emission as well as the location of the emitting exciton [28], the geometrical parameters differences between ground and excited state of DFP, TFP, FPZ, and OPZ are analyzed. Such as in DFP, the greatest changes bond lengths are observed on C_{p1}—N_2 and C_{p2}—N_2, which increase 0.018 Å from the ground state structures, and the inter-angles a(C_1—$C_{m'}$—C_m—C_{a2}) decreases from 79.7° to 76.0°. And in FPZ and OPZ, the largest increases bond lengths are C_{a1}—N_1 and C_{p1}—N_2 (about 0.021 Å). Interestingly, all the $C_{m'}$—C_m bond lengths of DFP, TFP, FPZ and OPZ in the excited state decrease in contrast to those of the ground state. It is obviously that the C—N_2, C—N_1 and $C_{m'}$—C_m are the parts of the molecule involved in light emission as well as the location of the emitting exciton.

On the basis of the excited-state geometries optimized by CIS method, TD-B3LYP/3-21G(d), TD-B3LYP/6-31G(d), TD-HF/3-21G(d) and TD-HF/6-31G(d) were used to predict emission spectra. The calculated results together with the experimental spectra [5,6] are summarized in Table 5. In general, the TD-HF will underestimate the excitation energies, but calculation results in Table 5 show the combination of TD-HF and CIS methods for excitation energies of these systems happen to be particularly balanced method in

Table 5
The fluorescence wavelengths calculated for all the meso-substituted porphyrins.

	Wavelengths (nm)				
	TD-B3LYP		TD-HF		Experiment [5,6]
	6-31G(d)	3-21G(d)	6-31G(d)	3-21G(d)	
DFP	545.9	535.2	721.7	645.9	640 and 704
TFP	556.8	544.8	730.4	653.9	662 and 725
FPZ	515.0	550.0	660.8	581.1	609 and 660
OPZ	520.9	556.5	662.2	581.7	614 and 661

describing emission energy in contrast to TD-B3LYP//CIS (the reason need to further investigate). Hence, the fluorescence spectra calculated by TD-HF are better than these values by TD-B3LYP. Furthermore, under the precondition, regulating basis set level up can also improve the accuracy of the fluorescent spectrum for the studied systems. Thus, the results of TDHF/6-31G(d) agree well with experimental values.

4. Conclusions

The electronic and optical properties of DFP, TFP, FPZ and OPZ have been investigated in this text. The main structures of porphyrin ring in them are similar. Among these compounds, the TFP molecule provides much easier hole injection, and OPZ provides much easier electron injection. Furthermore, FPZ has better equal rates of hole and electron transports than porphyrin (FBP), DPZ, TFP, and OPZ. Since the $\lambda_{electron}$ of DFP, TFP, FPZ and OPZ are smaller to that of tris(8-hydroxyquinolinato) aluminum(III), these molecules are generally regarded as the most promising electron transport materials. Experimental spectra are well recurred by theoretically investigation. The spectra overlap between the donor fluorescence (fluorene and fluorenone) and the acceptor absorption (DFP, TFP, FPZ and OPZ) spectra has been detected. This work attempts to provide some useful information for the charge carrier transport properties of new high efficiency red light-emitting material by theoretical investigations.

Acknowledgements

This work is supported by the Major State Basis Research Development Program (No. 2002CB613406), the National Natural Science Foundation of China (No. 20673045) and the State Key Laboratory for Superamolecular Structure and Material of Jilin University.

References

[1] C.W. Tang, S.A. VanSlyke, Appl. Phys. Lett. 51 (1987) 913.
[2] B.S. Li, J. Li, Y.Q. Fu, Z.S. Bo, J. Am. Chem. Soc. 126 (2004) 3430.
[3] B.S. Li, X.J. Xu, M.H. Sun, Y.Q. Fu, G. Yu, Y.Q. Liu, Z.S. Bo, Macromolecules 39 (2006) 456.
[4] S. Prathapan, S.I. Yang, J. Seth, M.A. Miller, D.F. Bocian, D. Holten, J.S. Lindsey, J. Phys. Chem. B 105 (2001) 8237.
[5] C.O. Paul-Roth, J.A.G. Williams, J. Letessier, G. Simonneaux, Tetrahedron Lett. 48 (2007) 4317.
[6] C.O. Paul-Roth, G. Simonneaux, C. R. Chimie 9 (2006) 1277.
[7] R.G. George, M. Padmanabhan, Polyhedron 22 (2003) 3145.
[8] S.I. Yang, J. Seth, J.P. Strachan, S. Gentemann, D. Kim, D. Holten, J.S. Lindsey, D.F. Bocian, J. Porphyr. Phthalocyanines 3 (1999) 117.
[9] R.A. Marcus, N. Sutin, Biochim. Biophys. Acta 811 (1985) 265.
[10] A. Ghosh, J. Am. Chem. Soc. 117 (1995) 4691.
[11] A. Ghosh, J. Phys. Chem. B 101 (1997) 3290.
[12] K.A. Nguyen, R. Pachter, J. Chem. Phys. 114 (2001) 10757.
[13] M. Stillman, J. Mack, N. Kobayashi, J. Porphyr. Phthalocyanines 6 (2002) 296.
[14] A.D. Becke, Phys. Rev. A 38 (1988) 3098.
[15] A.D. Becke, J. Chem. Phys. 98 (1993) 5648.
[16] C. Lee, W. Yang, R.G. Parr, Phys. Rev. B 37 (1988) 785.
[17] J.E. Ridley, M.C. Zerner, Theo. Chim. Acta 32 (1973) 111.
[18] M.J. Frisch, G.W. Trucks, H.B. Schlegel, G.E. Scuseria, M.A. Robb, J.R. Cheeseman, J.A. Montgomery, Jr., T. Vreven, K.N. Kudin, J.C. Burant, J.M. Millam, S.S. Iyengar, J. Tomasi, V. Barone, B. Mennucci, M. Cossi, G. Scalmani, N. Rega, G.A. Petersson, H. Nakatsuji, M. Hada, M. Ehara, K. Toyota, R. Fukuda, J. Hasegawa, M. Ishida, T. Nakajima, Y. Honda, O. Kitao, H. Nakai, M. Klene, X. Li, J.E. Knox, H.P. Hratchian, J.B. Cross, C. Adamo, J. Jaramillo, R. Gomperts, R.E. Stratmann, O. Yazyev, A.J. Austin, R. Cammi, C. Pomelli, J.W. Ochterski, P.Y. Ayala, K. Morokuma, G.A. Voth, P. Salvador, J.J. Dannenberg, V.G. Zakrzewski, S. Dapprich, A.D. Daniels, M.C. Strain, O. Farkas, D.K. Malick, A.D. Rabuck, K. Raghavachari, J.B. Foresman, J.V. Ortiz, Q. Cui, A.G. Baboul, S. Clifford, J. Cioslowski, B.B. Stefanov, G. Liu, A. Liashenko, P. Piskorz, I. Komaromi, R.L. Martin, D.J. Fox, T. Keith, M.A. Al-Laham, C.Y. Peng, A. Nanayakkara, M. Challacombe, P.M.W. Gill, B. Johnson, W. Chen, M.W. Wong, C. Gonzalez, J.A. Pople, Gaussian, Inc., Gaussian03, B.04 version, Pittsburgh, PA, 2003.
[19] G.S. Jiao, L.H. Thoresen, T.G. Kim, W.C. Haaland, F. Gao, M.R. Topp, R.M. Hochstrasser, M.L. Metzker, K. Burgess, Chem. Eur. J. 12 (2006) 7816.
[20] M. Gouterman, J. Chem. Phys. 30 (1959) 1139.
[21] S.F. Nelsen, F. Blomgren, J. Org. Chem. 66 (2001) 6551.
[22] G.R. Hutchison, M.A. Ratner, T.J. Marks, J. Am. Chem. Soc. 127 (2005) 2339.
[23] B.C. Lin, C.P. Cheng, Z.Q. You, C.P. Hsu, J. Am. Chem. Soc. 127 (2005) 66.
[24] W.D. Edwards, B. Weiner, M.C. Zerner, J. Am. Chem. Soc. 108 (1986) 2196.
[25] S.M. LeCours, S.G. DiMagno, M.J. Therien, J. Am. Chem. Soc. 118 (1996) 11854.
[26] J.S. Evans, R.L. Musselman, Inorg. Chem. 43 (2004) 5613.
[27] X. Zhou, A.M. Ren, J.K. Feng, Z.G. Shuai, J. Photochem. Photobiol. A: Chem. 172 (2005) 126.
[28] M.E. Köse, W.J. Mitchell, N. Kopidakis, C.H. Chang, S.E. Shaheen, K. Kim, G. Rumbles, J. Am. Chem. Soc. 129 (2007) 14257.